Calculation of the transfer efficiency between dual magneto-optical traps and simulation of a Ioffe trap for Bose–Einstein condensation

I. Yavin, T. Mikaelian, and A. Kumarakrishnan

Abstract: We consider the problem of transferring a cold atomic cloud from a low-vacuum chamber to an ultra-high-vacuum (UHV) chamber, where it can be recaptured and cooled to the transition temperature for Bose–Einstein condensation (BEC). Our calculation assumes an initial Maxwell–Boltzmann velocity distribution for the thermal cloud and a Gaussian spatial density distribution that is characteristic of magneto-optical traps (MOTs). Using a coordinate transformation we find the density of the recaptured atomic cloud as a function of time. This allows us to investigate the effect of experimental parameters on the transfer efficiency. These parameters include the distance of separation between the two chambers, the duration of the initial on-resonant laser used to push the thermal cloud, and the initial cloud temperature. We also present numerical simulations of the magnetic field due to a simplified Ioffe–Pritchard (IP) trap that has recently been used to obtain BEC using laser-cooling techniques. This trap converts a quadrupole magnetic field into an IP configuration using the magnetic field of a conical solenoid placed orthogonally to the axis of symmetry of a pair of quadrupole coils. Our results are suitable for small experimental groups interested in achieving BEC.

PACS No.: 03.75

Résumé : Nous étudions le problème du transfert d'un nuage d'atomes froids d'une chambre à vide bas vers une chambre à très haut vide (UHV), où il peut être recapturé et refroidi à la température de transition de la condensation de Bose–Einstein (BEC). Notre calcul suppose une distribution initiale de Maxwell–Boltzmann pour la vitesse des atomes froids et une distribution spatiale de Gauss pour la distribution de densité, ce qui est typique d'une trappe magnéto-optique. Utilisant une transformation de coordonnées, nous trouvons la densité de recapture du nuage atomique en fonction du temps. Ceci nous permet d'étudier l'effet des paramètres expérimentaux sur l'efficacité du transfert. Ces paramètres incluent la distance séparant les deux chambres, la durée de l'impulsion laser résonnante utilisée pour pousser le nuage, et la température initiale du nuage. Nous présentons également des simulations numériques du champ magnétique dû à une trappe simplifiée de Ioffe–Pritchard (IP), qui

Received 21 August 2002. Accepted 20 January 2003. Published on the NRC Research Press Web site at http://cjp.nrc.ca/ on 5 June 2003.

I. Yavin,[1] T. Mikaelian, and A. Kumarakrishnan.[2] Department of Physics and Astronomy, York University, 4700 Keele St., Toronto, ON M3J 1P3, Canada.

[1]Present address: Department of Physics, Harvard University, Cambridge, MA 02138, U.S.A.
[2]Corresponding author (e-mail: akumar@yorku.ca).

 doi: 10.1139/P03-050

a récemment été utilisée pour obtenir un BEC avec des techniques de refroidissement par laser. Cette trappe transforme un champ magnétique quadripolaire en une configuration IP en utilisant le champ magnétique d'un solénoïde conique placé orthogonalement à l'axe de symétrie d'une paire de bobines quadripolaires. Nos résultats peuvent être utiles pour de petits groupes expérimentaux désirant réaliser des BEC.

[Traduit par la Rédaction]

1. Introduction

A number of atomic systems have been recently Bose condensed using advances in laser cooling and magnetic trapping [1]. In these systems, the transition to Bose–Einstein condensation (BEC) occurs when a significant number of atoms accumulate in the ground state of a harmonic trapping potential. The condition for obtaining BEC is $n\lambda^3 \geq 2.612$ where n and λ are the density and thermal de-Broglie wavelength of the atoms, respectively. This condition was satisfied in a series of remarkable experiments [2–4] by starting with a large number of atoms in a magneto-optical trap (MOT) [5, 6] and using different techniques to rapidly increase the phase-space density. A relatively simple and efficient Ioffe–Pritchard (IP) trap was recently developed [7] to achieve BEC. This scheme involves the transfer of atoms from a low-vacuum MOT to a UHV MOT. The magnetic-field arrangement associated with the MOT overcomes some of the complexities of previous experiments and appears to be suitable for realization of BEC by small groups with limited resources. It is therefore crucial to understand the process of efficient atom transfer and the characteristics of the magnetic trap. This paper is organized as follows. Section 2 deals with the theoretical framework for the transfer of classical particles in a dual MOT arrangement. The results, shown in Sect. 3, allow us to investigate the effect of experimental parameters on the transfer efficiency. In Sect. 4, we discuss simulations of the magnetic-field arrangement and the advantages of this configuration.

2. Theoretical framework for atom transfer

Many BEC experiments use dual MOT configurations. This involves trapping atoms in a low-vacuum MOT ($\sim 10^{-8}$ Torr (1 Torr = 133.3 Pa)). This MOT is loaded from background vapor [6] using large diameter trapping beams to increase the capture velocity. Typically, this results in the capture of $\sim 10^9$ atoms with a temperature of ~ 100 μK [8]. The atoms are then transferred and recaptured in a MOT in a high-vacuum chamber ($\sim 10^{-11}$ Torr) to reduce collisions with thermal background atoms. The laser fields are then turned off to eliminate heating due to spontaneous emission and the trap is converted into a magnetic trap. BEC is then achieved by evaporative cooling [9] to the transition temperature ($\sim$100 nK).

We assume that the trapped atoms in the low-vacuum chamber have an isotropic Maxwell–Boltzmann velocity distribution and a spatially symmetric Gaussian spatial distribution. The normalized density is given by

$$n(\boldsymbol{r}, \boldsymbol{v}) = \frac{1}{\pi^3 r_0^3 v_0^3} \exp\left(-\frac{r_x^2 + r_y^2 + r_z^2}{r_0^2} - \frac{v_x^2 + v_y^2 + v_z^2}{v_0^2}\right) \tag{1}$$

where $v_0 = \sqrt{\frac{2KT}{m}}$ is the most probable speed and r_0 is the characteristic cloud radius. It is clear that one can write (1) as a product of exponents corresponding to each of the three directions

$$n(\boldsymbol{r}, \boldsymbol{v}) = \frac{1}{\pi^3 r_0^3 v_0^3} \exp\left(-\frac{r_x^2}{r_0^2} - \frac{v_x^2}{v_0^2}\right) \exp\left(-\frac{r_y^2}{r_0^2} - \frac{v_y^2}{v_0^2}\right) \exp\left(-\frac{r_z^2}{r_0^2} - \frac{v_z^2}{v_0^2}\right) \tag{2}$$

We define the origin of the coordinate system to coincide with the initial position of the center of the atomic cloud. Gravity acts along the negative $\hat{z}$ direction. The atoms can be transferred to the second

Fig. 1. Coordinate system (x, y, z) showing location of the initial cloud C, direction of on-resonant laser pulse L of duration T and region of recapture R defined by a cube of side $2D$. The dual MOT separation is l.

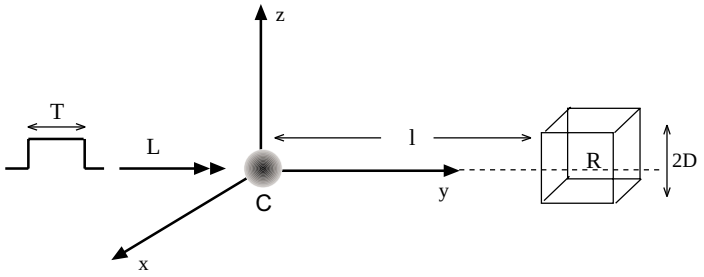

chamber, which is positioned at a horizontal distance l along the $\hat{y}$ direction, using an on-resonant laser pulse of duration T as shown in Fig. 1. We note that the atom transfer is usually accomplished in experiments using off-resonant counter-propagating laser beams. The frequencies of these laser beams are adjusted to compensate for the changing Doppler shift due to the acceleration. This ensures that the acceleration is constant during the transfer.

The experimental challenge is to maximize the percentage of atoms that can be recaptured in the second chamber. For a given separation l (usually determined by experimental constraints to be $\sim$0.5 m) the duration of the transfer pulse has to be adjusted appropriately. If the pulse duration is too long, the atoms will arrive in the second chamber with a velocity distribution such that the capture velocity of the UHV MOT coincides with the tail of the distribution. In this case, the fraction of captured atoms is small and multiple transfers are necessary to accumulate the desired number of atoms. The capture velocity is defined by the diameter of the trapping beams used in the second chamber [6,8]. If the pulse duration is too short, the cloud will fall under gravity and never reach the UHV chamber.

We now describe the steps involved in calculating the time-dependent density distribution of the atomic cloud trapped in the UHV chamber. We begin with (2) and transform it from a function of the initial position and velocity $(\boldsymbol{r}, \boldsymbol{v})$ to a function of time only. The acceleration in each direction is given by

$$\boldsymbol{a} = (0, a_l H(T - t), -g) \tag{3}$$

Here $a_l = \Gamma\hbar k/2m$ is the characteristic acceleration produced by the on-resonant pushing laser ($\Gamma = 1/\tau$ is the inverse of the transition life time and $k = 2\pi/\lambda$ is the wave vector for the atomic transition). We use the Heaviside function $H(T - t)$ to model the action of the laser for $0 < t < T$. It is unnecessary to consider the behavior of the Heaviside function for negative times since the derivation involves integrating the equation of motion over $t > 0$ only. Integration of (3) with respect to time from 0 to t yields

$$u_x = v_x \tag{4}$$

$$u_y = v_y + \int_0^t a_l H(T - t')\,\mathrm{d}t' = v_y + a_l(tH(T - t) + TH(t - T)) \tag{5}$$

$$u_z = v_z - gt \tag{6}$$

To obtain the time evolution of the position of the atoms, we integrate again with respect to time. This yields

$$x = r_x + v_x t \tag{7}$$

$$y = r_y + v_y t + \frac{1}{2}a_l t^2 H(T - t) + a_l t T H(t - T) - \frac{1}{2}a_l T^2 H(t - T) \tag{8}$$

$$z = r_z + v_z t - \frac{1}{2} g t^2 \tag{9}$$

The constants of integration are obtained by considering the initial values of position and velocity at $t = 0$. We can now use (4)–(9) to transform variables $(\boldsymbol{r}, \boldsymbol{v}) \rightarrow (x, z, t, \boldsymbol{u})$. Here y is fixed since it represents the position of the second chamber ($y = l$). Solving for $\boldsymbol{r}$ and $\boldsymbol{v}$ using (4)–(9) we obtain

$$v_x = u_x \tag{10}$$

$$v_y = u_y - a_l(tH(T-t) + TH(t-T)) \tag{11}$$

$$v_z = u_z + gt \tag{12}$$

$$r_x = x - u_x t \tag{13}$$

$$r_y = y - u_y t + \frac{1}{2} a_l t^2 H(T-t) + \frac{1}{2} a_l T^2 H(t-T) \tag{14}$$

$$r_z = z - u_z t - \frac{1}{2} g t^2 \tag{15}$$

Using this transformation we can calculate the Jacobian to be

$$\begin{aligned} J &= \left| \frac{\partial(\boldsymbol{r}, \boldsymbol{v})}{\partial(x, z, t, \boldsymbol{u})} \right| \\ &= \begin{vmatrix} 1 & 0 & -u_x & -t & 0 & 0 \\ 0 & 0 & -u_y + a_l t H(T-t) - \frac{1}{2} a_l t^2 \delta(t-T) + \frac{1}{2} a_l T^2 \delta(t-T) & 0 & -t & 0 \\ 0 & 1 & -u_z - gt & 0 & 0 & -t \\ 0 & 0 & 0 & 1 & 0 & 0 \\ 0 & 0 & -a_l H(T-t) - t\delta(t-T) + T\delta(t-T) & 0 & 1 & 0 \\ 0 & 0 & g & 0 & 0 & 1 \end{vmatrix} \\ &= u_y \end{aligned} \tag{16}$$

Here, δ refers to the Dirac delta function. Substituting (10)–(15) into (2) and multiplying by the Jacobian we obtain the density as a function of $(x, z, t, \boldsymbol{u})$

$$\begin{aligned} n(x, z, t, \boldsymbol{u}) = \frac{1}{\pi^3 r_0^3 v_0^3} \exp\left(-\frac{(x - u_x t)^2}{r_0^2} - \frac{u_x^2}{v_0^2} \right) \\ \times \exp\left(-\frac{(y - u_y t + \frac{1}{2} a_l t^2 H(T-t) + \frac{1}{2} a_l T^2 H(t-T))^2}{r_0^2} \right. \\ \left. - \frac{(u_y - a_l(tH(T-t) + TH(t-T)))^2}{v_0^2} \right) \\ \times \exp\left(-\frac{(z - u_z t - \frac{1}{2} g t^2)^2}{r_0^2} - \frac{(u_z + gt)^2}{v_0^2} \right) \times u_y \end{aligned} \tag{17}$$

However, we are interested in the atomic density as a function of time only. Since only atoms arriving at the UHV trap ($y = l$) with a velocity less than the capture velocity u_0 will be trapped, we have to integrate $\boldsymbol{u}$ over a finite range. Since we assume a square cross section for the UHV trap at $y = l$, we have to integrate over x and z as well. This can be written as

$$n(t) = \int_{-D}^{D} \mathrm{d}x \int_{-D}^{D} \mathrm{d}z \iiint_{-u_0}^{u_0} n(x, z, t, u_x, u_y, u_z)\, \mathrm{d}^3 u \tag{18}$$

The integral over x and z can be done analytically and expressed in terms of error functions using symbolic computation programs such as Maple. The result can be evaluated numerically to obtain the fraction of atoms trapped in the second MOT chamber as a function of time.

Fig. 2. $n(t)$ versus t for $T = 173\ \mu$s, $v_0 = 0.167$ m/s, $l = 0.5$ m, $D = 0.01$ m, and $u_0 = 20$ m/s.

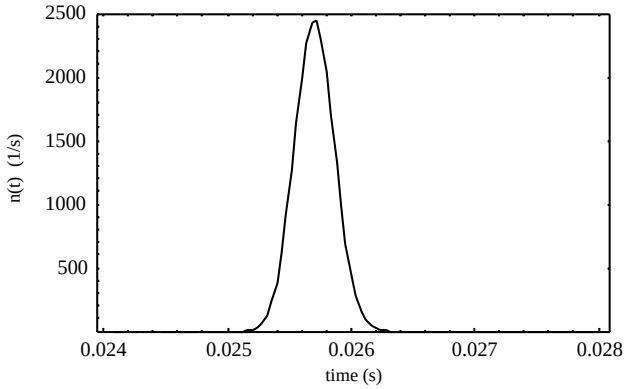

Fig. 3. Transfer efficiency versus the pulse duration T.

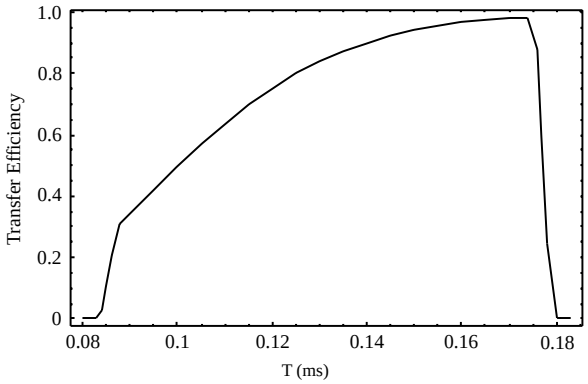

3. Results of the theoretical model

Figure 2 shows the probability density as a function of time given by (18). Here we have assumed parameters typical of a dual MOT system for rubidium atoms. We assume the distance of separation between traps to be $l = 0.5$ m. This separation allows for the flexible design of the UHV MOT. Here we have assumed a $v_0 = 0.167$ m/s, which corresponds to the Doppler limit [10] for two level Rb atoms (we note that this temperature is similar to the typical temperature in a MOT and has no particular significance). The atoms are transferred by the on-resonance laser pulse of duration $T = 173\ \mu$s, with acceleration of $a_l = 1.12 \times 10^5$ m/s^2. The initial size of the cloud is $r_0 = 1$ mm. We assume that the dimension of the trapping beams in the second chamber are such that $D = 10$ mm and the capture speed is $u_0 = 20$ m/s. This capture speed is comparable to the typical value obtained in experiments. We note that the peak in Fig. 2 occurs at $t = 0.0256$ s. This is consistent with the intuitive expectation that the peak will occur at $t_{\text{peak}} = l/a_l T$. It can also be shown that the width of the distribution is given by $\Delta t \sim t_{\text{peak}} v_0/a_l T + r_0/a_l T$, which is consistent with our results. For the parameters assumed above, the width of the curve depends more strongly on the initial velocity distribution than on the initial cloud size. By integrating the probability density over time, we obtain the fraction of atoms transferred to the second chamber to be 0.98. Our results show that it is feasible to acquire a sufficient number of atoms for the stages involved in the BEC experiment after a single transfer from the low-vacuum MOT. This can be explained by noting that the cloud has dropped under gravity by approximately $gt_0^2/2 = 3.2$ mm, which is smaller than the radius of the trapping beams ($\sim$1 cm) in the UHV MOT. Figure 3 shows the transfer fraction as a function of the pulse duration T. As noted in the previous section, the fraction decreases rapidly if the speed of the atom cloud approaches the capture speed (pulse duration is too

Fig. 4. Schematic diagram of a simple IP trap configuration. The y axis is directed positively into the page.

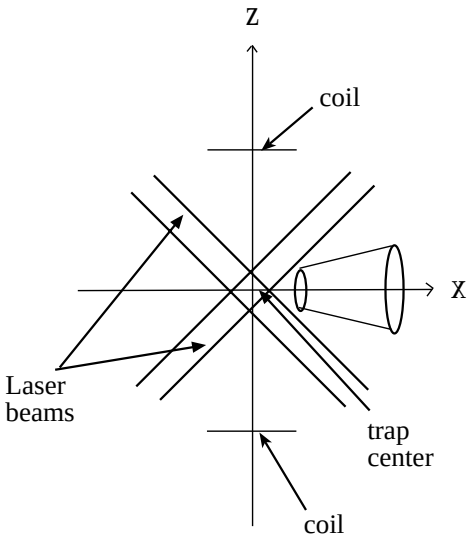

large) or as the cloud is displaced significantly under gravity and is unable to reach the volume define by the trapping beams of the UHV MOT (pulse duration is too short).

4. Simulation of a modified Ioffe trap

After transferring the atoms to the UHV MOT, the trap can be converted to a purely magnetic trap. Evaporative cooling is then necessary to reach the BEC transition temperature. We now discuss a simulation, a relatively simple and efficient IP trap that was recently developed [7]. This magnetic trap overcomes some of the experimental complexities of other traps and appears to be suitable for realization of BEC by small groups with limited resources. The coil configuration for this trap consists of two quadrupole coils with opposing currents, and a tapered conical solenoid placed with its axis at right angles to the axis of symmetry of the quadrupole coils (see Fig. 4). All coils can be placed outside the vacuum chamber, reducing experimental difficulties. The taper on the conical solenoid allows optical access for the trapping beams although the edge of the cone is placed close to the center of the MOT. When the current in the conical solenoid is switched on, the initial quadrupole trap is adiabatically converted to an IP trapping field with a nonzero minimum. This ensures efficient transfer of atoms from the UHV MOT to the IP trap. The center of the IP trap is only a few millimetres from the center of the MOT, reducing difficulties associated with alignment. In addition, the IP trap offers good confinement and requires relatively modest operating currents ($\sim$25 A). Atoms transferred to the IP trap can be Bose condensed using RF evaporation.

The magnetic trapping force depends on the interaction between the magnetic moment of the atom and the magnetic field. This force is given by

$$\boldsymbol{F} = \nabla(\boldsymbol{\mu} \cdot \boldsymbol{B}) \tag{19}$$

where the magnetic moment μ is related to the magnetic quantum number. Majorana transitions are a significant problem associated with magnetic traps at locations where the magnitude of the magnetic field is zero. Such transitions occur whenever the magnetic moment of an atom cannot maintain its orientation with respect to the magnetic-field lines. To avoid such Majorana transitions, the Larmor precession rate ω_{L} of the atom's magnetic moment around the magnetic field must exceed the rate of change of the magnetic field experienced by the atom due to the motion in the trapping field. Atoms in

a particular magnetic sublevel undergo Majorana transitions and evolve into other magnetic sublevels. The magnetic moments of these sublevels correspond to untrapped states. The problem of Majorana transitions is known [11] to become crucial at very low temperatures, typical of BEC experiments. At these temperatures, the trajectories of the atoms will mostly be in the central minimum region of the potential well, where the magnetic field is zero. Thus, there will be a considerable leakage of atoms at the trap center.

A simple magnetic trap such as a quadrupole trap [12,13] consists of two coils with equal opposing currents. Near the center, the field varies linearly as a function of position. The trapped atoms are localized at the central minimum of the trap, where the magnetic field is zero. As the temperature is lowered, a significant number of these atoms are expelled from the trap.

An IP trap is usually constructed from a set of four bars with a current flowing in opposite directions through each pair of bars. The bars, which provide the radial field gradient, are placed within two circular coils carrying the current in the same direction. The circular coils provide axial confinement and ensure a nonzero minimum field. The disadvantages of a typical IP trap are high power dissipation in the coils and experimental difficulties associated with aligning the centers of the MOT and the IP trap. In addition, the "Ioffe bars" reduce optical accessibility.

Several ingenious solutions [3,9,13–15] have been devised to prevent Majorana transitions in BEC experiments. These solutions involve various IP traps with nonzero minima, the design of the TOP trap, and the introduction of a repulsive optical potential at the vicinity of the zero of the magnetic field.

We now discuss the details of the coil configuration for the newly proposed IP trap [7]. A schematic diagram of this trap is shown in Fig. 4. The anti-Helmholtz coils are placed coaxially along the z axis. The conical solenoid is placed along the x axis as shown. We use the same parameters as in ref. 7: the anti-Helmholtz coils have 180 turns and an average radius of 25.5 mm. Their centers are 66 mm apart. The conical coil consists of 150 turns. The smallest radius of the cone is 3 mm, and the largest radius is 15 mm. The length of the cone is 34 mm (half of the cone angle is $\sim$19.4°). The center of the cone is 34 mm from the origin O of our coordinate system. For the purpose of our calculations, we ignore the length of the anti-Helmholtz coils. We use the average radii of the coils, ignoring the coil thickness. For the sake of simplicity, we also assume that the conical solenoid consists of a single layer of turns.

4.1. Magnetic field of the anti-Helmholtz coils

For the anti-Helmholtz coils, the magnetic field at a general point in space can be calculated using the Biot–Savart law. Figure 4 shows the Cartesian coordinate system. Here, the z axis is the symmetry axis of the coils. Let R be the radius of the coils and d be the distance of separation. The magnetic field due to the first coil at $z = -d/2$ can be calculated as follows. We assume that $\boldsymbol{r} = x\hat{i} + y\hat{j} + z\hat{k}$ is the position vector of the point where the magnetic field is to be calculated. $\boldsymbol{r}' = R\cos(s)\hat{i} + R\sin(s)\hat{j} - (d/2)\hat{k}$ represents a point on the rim of the coil; s is an angular parameter changing from 0 to 2π along the coil. We therefore have

$$\mathrm{d}\boldsymbol{r}' = -R\sin(s)\,\mathrm{d}s\hat{i} + R\cos(s)\,\mathrm{d}s\hat{j}$$

$$\boldsymbol{r} - \boldsymbol{r}' = (x - R\cos(s))\hat{i} + (y - R\sin(s))\hat{j} + \left(z + \frac{d}{2}\right)\hat{k}$$

and

$$\|\boldsymbol{r} - \boldsymbol{r}'\| = \sqrt{x^2 + y^2 + R^2 - 2xR\cos(s) - 2yR\sin(s) + \left(z + \frac{d}{2}\right)^2}$$

Furthermore,

$$\mathrm{d}\boldsymbol{r}' \times (\boldsymbol{r} - \boldsymbol{r}') = \left(\left(z + \frac{d}{2}\right)(R\cos(s))\,\mathrm{d}s\right)\hat{i} + \left(\left(z + \frac{d}{2}\right)(R\sin(s))\mathrm{d}s\right)\hat{j} + ((R^2 - Ry\sin(s) - Rx\cos(s))\mathrm{d}s)\hat{k}$$

The magnetic field due to the coil at $z = -d/2$ is given by

$$\boldsymbol{B}_-(\boldsymbol{r}) = \frac{\mu_0 I N}{4\pi}\int_0^{2\pi} \frac{\mathrm{d}\boldsymbol{r} \times (\boldsymbol{r} - \boldsymbol{r}')}{\|\boldsymbol{r} - \boldsymbol{r}'\|^3}$$

A similar analysis as the above can be performed for the second coil, placed at $z = d/2$ to obtain $\boldsymbol{B}_+(\boldsymbol{r})$. By the superposition principle, the total field due to both coils is

$$\begin{aligned}\boldsymbol{B}(\boldsymbol{r}) &= \boldsymbol{B}_-(\boldsymbol{r}) + \boldsymbol{B}_+(\boldsymbol{r}) \\ &= \frac{\mu_0 I N}{4\pi}\int_0^{2\pi} \frac{\left(z + \frac{d}{2}\right)\left(\hat{i}R\cos(s) + \hat{j}R\sin(s)\right) + \left(R^2 - Ry\sin(s) - Rx\cos(s)\right)\hat{k}}{\left(x^2 + y^2 + R^2 - 2xR\cos(s) - 2yR\sin(s) + \left(z + \frac{d}{2}\right)^2\right)^{3/2}}\mathrm{d}s \\ &+ \frac{\mu_0(-I)N}{4\pi}\int_0^{2\pi} \frac{\left(z - \frac{d}{2}\right)\left(\hat{i}R\cos(s) + \hat{j}R\sin(s)\right) + \left(R^2 - Ry\sin(s) - Rx\cos(s)\right)\hat{k}}{\left(x^2 + y^2 + R^2 - 2xR\cos(s) - 2yR\sin(s) + \left(z - \frac{d}{2}\right)^2\right)^{3/2}}\mathrm{d}s\end{aligned}$$

where $\mu_0 = 4\pi \times 10^{-7}$ T m/A is the permeability, I is the current, and N is the number of turns in each coil. Setting $y = z = 0$ gives the field of the anti-Helmholtz coils along the x axis (symmetry axis of the cone). It is given by

$$B_x(x, 0, 0) = \frac{IdN\mu_0}{\pi}\frac{\left((8Rx)^2 + m^2\right)K[a] + m(m - Rx)E[a]}{x\sqrt{m - 8Rx}(d^4 + 8d^2R^2 + 16R^4 + 8d^2x^2 - 32R^2x^2 + 16x^4)} \tag{20}$$

where $m = d^2 + 4R^2 + 4x^2$, and K and E are complete elliptic integrals defined as

$$K[a] = \int_0^{2\pi} \frac{\mathrm{d}\theta}{\sqrt{1 - a^2\sin^2\theta}}$$

$$E[a] = \int_0^{2\pi} \sqrt{1 - a^2\sin^2\theta}\,\mathrm{d}\theta$$

The argument a of the elliptic integrals K and E is given by

$$a = -\frac{16Rx}{d^2 + 4R^2 - 8Rx + 4x^2}$$

Figure 5 shows a plot of (20), which gives the magnetic field of the anti-Helmholtz coils for a current of 25 A (field gradient ~144 G/cm at the origin). The field varies linearly between the coils and is zero at the origin, midway between the coils.

4.2. Magnetic field of the conical solenoid

The magnetic field of a single loop of wire along its axis of symmetry can also be obtained from the Biot–Savart law, and is given by

$$B_c = \frac{IR^2\mu_0}{2\left(R^2 + x^2\right)^{3/2}}$$

Fig. 5. Magnetic field of the anti-Helmholtz coils at a current of 25 A.

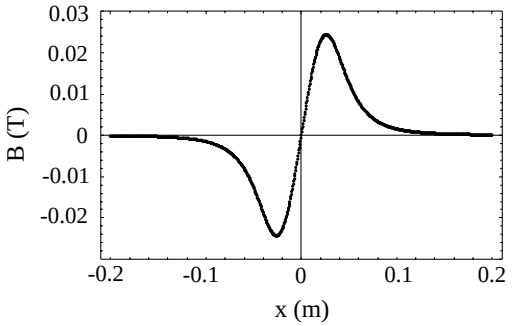

Fig. 6. Magnetic field of the conical solenoid at a current of 27 A.

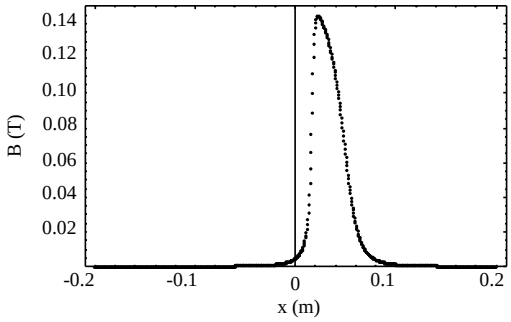

Fig. 7. Total trapping field.

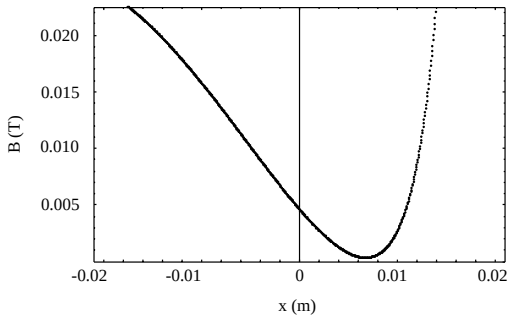

where x is the distance from the center of the coil, R is the radius of the coil, and I is the current through the coil. The cone's magnetic field is obtained by adding up the fields due to the individual loops constituting the conical solenoid. The increment $\mathrm{d}R$ used for the radius is given by $\mathrm{d}R = (R_2 - R_1)/N$, where R_2 and R_1 are the largest and the smallest radii of the cone, respectively, and N is the total number of turns. The corresponding increments in the distance from the coil to a point where the field is to be calculated scale as $\mathrm{d}R/\tan(\alpha)$, where α is the half angle of the cone. Figure 6 shows a plot of the cone's field along its axis, when a current of 27 A is used. Qualitatively, the cone's field exhibits a peak close to the center of the anti-Helmholtz coils. The variation of the magnetic field with respect to the peak is not symmetric. The field diminishes more rapidly near the tapered end of the cone. The total field can be obtained using the superposition principle. Figure 7 shows the resultant trapping field. It can be seen that the two individual fields nearly cancel at $x \sim 7$ mm, and a nonzero minimum is formed, similar to an IP trapping field. It should be noted that adding a uniform field to the quadrupole configuration of Fig. 5 will only shift the position where the magnetic field is zero, i.e., it is not possible to eliminate the zero of the magnetic field by using a uniform bias field.

4.3. Results of the trapping magnetic-field simulation

The absolute value of the magnetic field of the IP trap is plotted in Fig. 8, as a function of current through the conical coil. The current through the anti-Helmholtz coils is kept constant at 25 A, as in ref. 7. Figure 8*a* represents the field of the anti-Helmholtz configuration. Since adding a uniform field shifts the zero of the quadrupole field, it is expected that initially the magnetic field of the conical solenoid, although nonuniform, will shift the zero slightly from the center of the trap and towards the cone. This is illustrated in Figs. 8*b* through 8*d*. Increasing the current through the conical solenoid results in two minima in the trapping potential. It is therefore possible to transfer atoms adiabatically

Fig. 8. Magnetic field of the IP trap for increasing current through the conical solenoid. The current through the anti-Helmholtz coils is 25 A; the current through the cone is (*a*) 0 A, (*b*) 10 A, (*c*) 15 A, (*d*) 20 A, (*e*) 27 A.

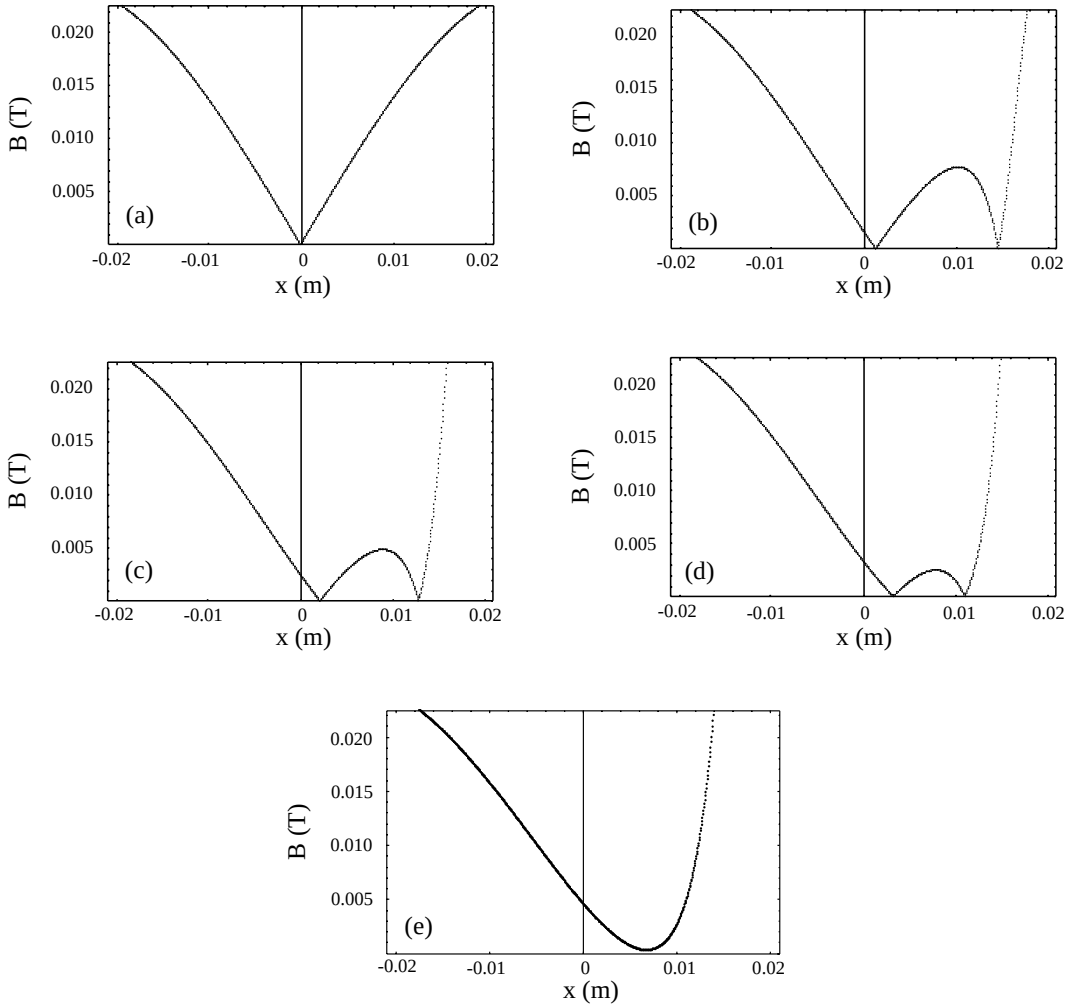

to the newly formed minimum in the trapping potential. The cone's field varies rapidly with position so that the anti-Helmholtz field is almost cancelled at a spatial location very near the center of the MOT. At a current of about 27 A through the cone, the two minima combine into a single nonzero minimum. The result is the asymmetric potential trap shown in Fig. 8*e*. It can be shown that the field gradient increases more rapidly toward the cone under these conditions and that atoms will be localized in a central elongated region near the minimum. It can also be seen that the potential in Fig. 8*e* is nonzero and that its minimum is shifted by $\sim$7 mm away from the center of the UHV MOT toward the center of the conical solenoid. Since this is sufficiently close to the center of the trap, the loss of atoms during the transfer from the MOT to the magnetic trap is reduced. This field provides a stable magnetic trap (quadratic potential near the minimum), which is a prerequisite for RF-induced evaporative cooling. Our results are in excellent agreement with those given in ref. 7. Finally, we note that the these results were obtained from first principles and modelled using standard mathematical software such as Mathematica and Maple, whereas the authors of ref. 7 used dedicated commercial software.

5. Conclusions

In summary, we have used a transparent technique involving a coordinate transformation to calculate the fraction of atoms that can be transferred from a low-vacuum MOT to a second chamber where they are recaptured. The calculation allows for the flexible design of a UHV MOT that can be easily attached to an existing MOT apparatus. We find that it is possible to achieve a transfer efficiency of the order of unity. In practice, however, the transfer efficiency in experiment will be limited by factors such as, the size of the aperture used to maintain the differential pressure between the two vacuum chambers, the distance of the aperture from the low-vacuum MOT and the wave-front quality of the laser beams used for pushing and recapturing the cloud. However, the transfer efficiency calculated in this paper is comparable to the value that has been obtained in various experiments [16]. The results of our magnetic-field simulations can be used to design a low-cost Ioffe trap suitable for small groups interested in achieving BEC. The simulations can be easily adapted to rescale the apparatus to suit experimental conditions. The technique employed is quite a general one and can be used for a number of applications such as a calculation of the time-of-flight signal of trapped atoms [17]. Other applications could involve a calculation of the transfer efficiency of atoms into beam-loaded traps.

Acknowledgments

This research is supported by the Canada Foundation for Innovation, Ontario Innovation Trust, York University, and the Natural Sciences and Engineering Research Council of Canada.

References

1. H.R. Sadghpour, D.E. Pritchard, and E.J. Heller (*Editors*). Proceedings XVIII International Conference on Atomic Physics. 2002. World Scientific, Singapore. 2002.
2. M.H. Anderson, J.R. Ensher, M.R. Matthews, C.E. Wieman, and E.A. Cornell. Science (Washington), **269**, 198 (1995).
3. K.B. Davis, M.O. Mewes, M.R. Andrews, N.J. van Druten, D.S. Durfee, D.M. Kurn, and W. Ketterle. Phys. Rev. Lett. **75**, 3969 (1995).
4. C.C. Bradley, C.A. Sackett, and R.G. Hulet. Phys. Rev. Lett. **78**, 985 (1997).
5. E.L. Raab, M. Prentiss, A. Cable, S. Chu, and D.E. Pritchard. Phys. Rev. Lett. **59**, 2631 (1987).
6. C. Munroe, W. Swann, H. Robinson, and C. Wieman. Phys. Rev. Lett. **65**, 1571 (1990).
7. T. Esslinger, I. Bloch, and T.W. Hänsch. Phys. Rev. A: At. Mol. Opt. Phys. **58**, R2664 (1998).
8. K.E. Gibble, S. Kasapi, and S. Chu. Opt. Lett. **17**, 526 (1992).
9. W. Petrich, M.H. Anderson, J.R. Ensher, and E.A. Cornell. Phys. Rev. Lett. **74**, 3352 (1995).
10. P.D. Lett, W.D. Phillips, S.L. Rolston, C.E. Tanner, R.N. Watts, and C.I. Westbrook. J. Opt. Soc. Am. B, **6**, 2084 (1989).
11. W. Ketterle, D.S. Durfee, and D.M. Stamper-Kurn. Bose-Einstein condensation in atomic gases: Proceedings of the International School of Physics "Enrico Fermi". Varenna on Lake Como. 7–17 July 1998. *Edited by* M. Inguscio, S. Stringari, and C.E. Wieman. IOS Press, Amsterdam; Ohmsha, Tokyo. 1999.
12. A.L. Migdall, J.V. Prodan, W.D. Phillips, T.H. Bergeman, and H.J. Metcalf. Phys. Rev. Lett. **54**, 2596 (1985).
13. T. Bergeman, G. Erez, and H.J. Metcalf. Phys. Rev. A: Gen. Phys. **35**, 1535 (1987).
14. M.-O. Mewes, M.R. Andrews, N.J. van Druten, D.M. Kurn, D.S. Durfee, and W. Ketterle. Phys. Rev. Lett. **77**, 416 (1996).
15. C.J. Myatt, E.A. Burt, R.W. Ghrist, E.A. Cornell, and C.E. Wieman. Phys. Rev. Lett. **78**, 586 (1997).
16. T.B. Swanson, D. Asgeirsson, J.A. Behr, A. Gorelov, and D. Melconian. J. Opt. Soc. Am. B, **15**, 2641 (1998) and refs. therein.
17. I. Yavin, M. Weel, A. Andreyuk, and A. Kumarakrishnan. Am. J. Phys. **70**, 149 (2002).